Mesoporous Crystals

DOI: 10.1002/ange.200601451

A Lesson from the Unusual Morphology of Silica Mesoporous Crystals: Growth and Close Packing of Spherical Micelles with Multiple Twinning**

*Keiichi Miyasaka, Lu Han, Shunai Che, and Osamu Terasaki**

Ordered mesoporous silicas synthesized through the self-assembly of amphiphilic surfactants are of great interest because of their potential for new applications, for which the control of particle shape and size are vital. Some mesoporous crystals show characteristic morphology, such as MCM-48 crystals ($Ia\bar{3}d$) with truncated rhombic dodecahedra;[1] HMM-3/SBA-1 ($Pm\bar{3}n$) with well-defined decaoctahedra[2,3] and 74 faces as well as 54 faces with crystal-like shape;[4] SBA-7 ($P6_3/mmc$) with 20 distinct crystal faces with one sixfold axis;[5] and FDU-1 ($Im\bar{3}m$) with rhombododecahedra.[6] Furthermore, morphological evolution of SBA-1 was investigated with respect to various synthetic parameters such as temperature, acidity, time, concentration, and so on.[7] All morphologies reported in the above references were commensurate with crystallographic point-group symmetries, and were observed from the crystals synthesized under well-controlled conditions for crystal growth processes.

Recently, we have synthesized a crystal that shows a well-resolved powder X-ray diffraction (XRD) profile, but its morphology does not fit any crystallographic point-group symmetry. Herein, we present a structural solution for a well-ordered mesoporous silica crystal of the cage type with cubic $Fm\bar{3}m$ symmetry, and its structural description for the morphologies involved. The study was performed by powder XRD, scanning electron microscopy (SEM), and high-resolution transmission electron microscopy (HRTEM). Morphologies such as an icosahedron or a decahedron of cubic $Fm\bar{3}m$ structure seem to be inconsistent with the corresponding point-group symmetry, $m\bar{3}m$. However, the structure is explained in terms of the occurrence of multiple twinning during the formation of mesostructures. This behavior has been observed for face-centered cubic (FCC) metals.

Highly ordered mesoporous silica was prepared using the gemini cationic surfactant, $C_{16\text{-}3\text{-}1}$ (see Experimental Section), as template with a very low surfactant concentration of 0.36 wt %. The surfactant $C_{16\text{-}3\text{-}1}$ has two head groups and one tail, which makes the effective area of the critical packing parameter larger than that of normal surfactants used for conventional mesoporous silicas. Therefore, micelles form a lyotropic, liquid-crystal mesophase with high curvatures. Figure 1 shows the XRD pattern of the calcined sample,

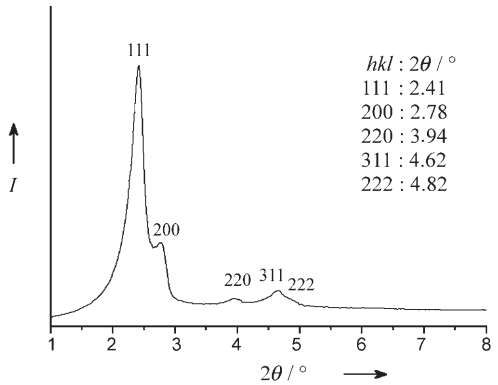

Figure 1. Powder XRD pattern of the calcined silica mesoporous crystal recorded in the region of $2\theta = 1.0$–$8.0°$. The pattern was indexed assuming a cubic lattice.

which is indexable with the cubic lattice, as supported by the TEM observations discussed below. The pattern shows two well-resolved sharp peaks indexed as 111 and 200 reflections in the region of $2\theta = 1.5$–$3.0°$, and three additional weak peaks indexed as 220, 311, and 222 reflections in the range of $2\theta = 3.5$–$6.0°$. The unit cell parameter a is 63 Å. The nitrogen adsorption–desorption isotherm of this sample is provided in the Supporting Information, together with the pore-size distribution analysis using nonlocal density functional theory. The Brunauer–Emmett–Teller (BET) surface area and the total pore volume are 778 $m^2 g^{-1}$ and 0.345 $cm^3 g^{-1}$, respectively. In the isotherm, the capillary condensation step observed at lower relative pressure ($P/P_0 < 0.2$) is analogous to that of high-quality MCM-41 with small pores templated by short-chain surfactants.

SEM images showed unusual morphologies from the point-group symmetry $m\bar{3}m$ expected from the space-group symmetry $Fm\bar{3}m$. Such morphologies can be categorized into two types: "plate" and "polyhedron" (see Figure 2a,b). The plate category normally showed a threefold triangular shape truncated at its vertices. For the polyhedron category, an icosahedral shape was typically observed. For the observed shapes of relevance, decahedral, Wulff, and D-Wulff polyhedrons can be categorized (see Figure 2c–e), although these were observed less often. The particle size of the icosahedron tended to be relatively smaller ($< 10\,\mu m$) than that of the other shapes, where plate-type particles show a variety of

[*] K. Miyasaka, Prof. O. Terasaki
Structural Chemistry, Arrhenius Laboratory
Stockholm University
10691 Stockholm (Sweden)
Fax: (+46) 816-3118
E-mail: terasaki@struc.su.se
L. Han, Prof. S. Che
School of Chemistry and Chemical Technology
State Key Laboratory of Composite Materials
Shanghai Jiao Tong University
800 Dongchuan Road, Shanghai, 200240 (P.R. China)

[**] O.T. thanks the Swedish Science Research Council (VR) and the Japan Science and Technology Agency (JST) for financial support. This work was also supported by the National Natural Science Foundation of China (Grant Nos. 20425102 and 20521140450), the China Ministry of Education, and the Shanghai Science Foundation (0452nm061 and 05XD14010).

Supporting information for this article is available on the WWW under http://www.angewandte.org or from the author.

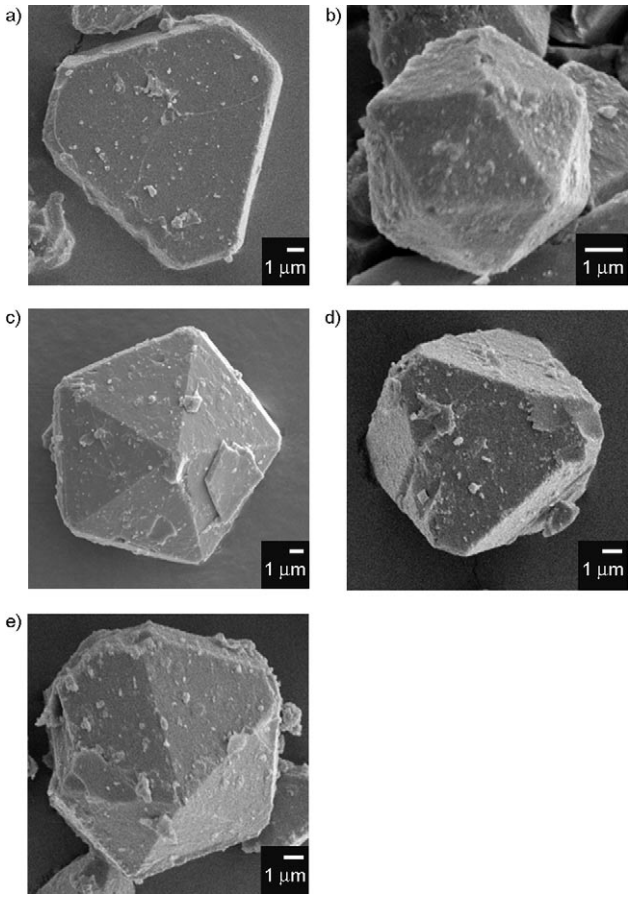

Figure 2. Typical SEM images of calcined silica mesoporous crystals coated by gold. a) Particle of plate type; its vertices are often truncated. b) Icosahedral shape. c) Decahedral shape. d) Particle showing the Wulff polyhedron. e) Particle showing the D-Wulff polyhedron.

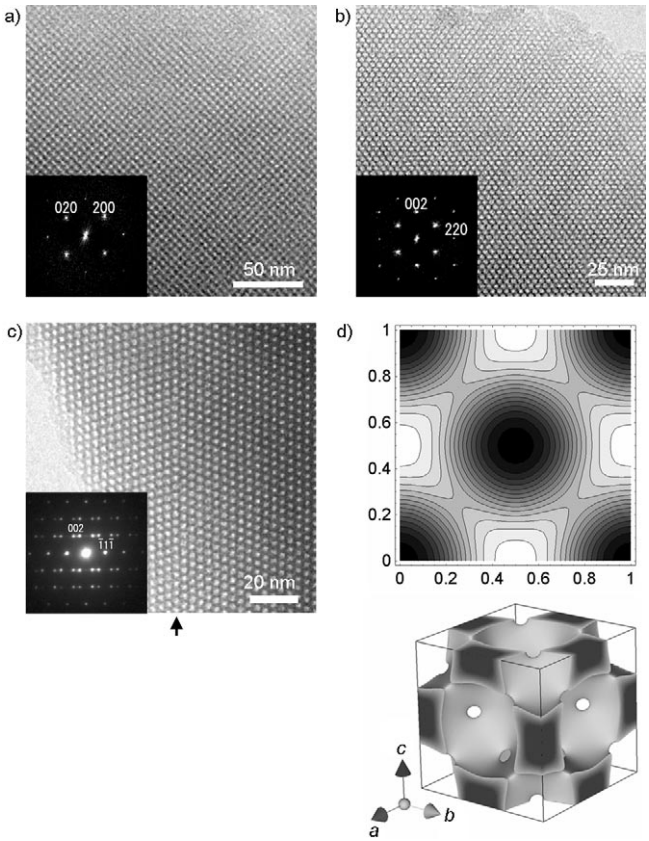

Figure 3. HRTEM images with the corresponding Fourier diffractograms inset, taken from a) [001] and b) [110] incidence. c) HRTEM image showing an occasional single twin boundary (indicated by an arrow) observed along [110]. The corresponding ED pattern (inset) is indexed based on the rightward region. d) The resultant structure of the calcined silica mesoporous crystal through the electron crystallographic process. Top: contour plot sliced perpendicular to [001] at $z=0$, where white and black correspond to the silica wall and the pore, respectively. Bottom: 3D representation of one unit cell of the crystal with $Fm\bar{3}m$ symmetry.

sizes up to 20 μm and decahedral particles sit around 10 μm. These morphological features will be discussed later in combination with the TEM results.

HRTEM images of the crystal demonstrate the pore arrangement covering a large area with beautiful crystallinity (see Figure 3a,b). We observed the sequential presence of four-, two-, and sixfold rotational symmetries in the projected images taken with [100], [110], and [111] incidences by tilting the specimen. The reflection conditions derived from the Fourier diffractograms of the HRTEM images are summarized as $\{hkl: h+k, k+l, l+h=2n; 0kl: k, l=2n; hhl: h+l=2n; 00l: l=2n\}$, which provide the possible space groups $F432$ (No. 209), $F\bar{4}3m$ (No. 216), and $Fm\bar{3}m$ (No. 225). However, the first option is excluded when taking into account the Wulff polyhedral single crystal observed (Figure 2d), because the symmetry group of a regular octahedron is $S_4 \times C_2$ which the first option does not possess. We conclusively chose $Fm\bar{3}m$ rather than $F\bar{4}3m$ because of its higher symmetry. Twinnings are occasionally observed in the image. A typical image is shown in Figure 3c, with the inset showing the electron diffraction (ED) pattern taken from the corresponding selected area. In this image, it is clear that there is merely a single twin boundary halving the field (indicated by an arrow).

Fourier analysis of HRTEM images based on electron crystallography was performed to elucidate the structural details, such as the pore shape and the possible pore connectivity. The details of the process can be found elsewhere.[3,8] The resultant Fourier coefficients (FCs) are tabulated in the Supporting Information. The electrostatic potential distribution, $\rho(x,y,z)$, is three-dimensionally built by Fourier synthesis from a set of FCs by taking into account $Fm\bar{3}m$ symmetry [Eq. (1)].

$$\rho(x,y,z) = \sum_{hkl} F_{hkl} \cos(2\pi h x) \cos(2\pi k y) \cos(2\pi l z) \quad (1)$$

The contour plot for the plane of $\rho(x,y,z)$ sliced at $z=0$, perpendicular to [001], is shown in Figure 3d together with a three-dimensional (3D) structural representation. We took the crystallographic origin at the center of the cage. One cage has 12 nearest neighbors. Mesocaged porous silicas comprising a cubic close-packed (CCP) arrangement have been reported previously, for example, as SBA-2[9] and SBA-12.[10]

It is known that CCP stacking of spherical micelles stays next to hexagonal close-packed (HCP) stacking, and the HCP domain is often found in HRTEM images in the literature as random mixtures of both stacking (SBA-2) and segregated domains (SBA-12). In comparison with these, our sample showed overwhelming CCP over HCP stacking, and HCP stacking was observed only at the twin boundaries. The effect of HCP stacking on the XRD pattern as a result of twinning will be discussed below in terms of the formation of the particles and their size.

Nowadays the morphologies included herein are known as a remarkable feature of FCC crystals. A plate can be explained by the presence of single twinning in a tetrahedral/octahedral single FCC crystal (see Figure 4a), whilst particular polyhedrons can be multiply twinned particles (MTPs). The MTP model was first introduced by Ino[11] in the 1960s. It was applied to the epitaxial growth of metal particles and successfully explained the presence of the icosahedral or decahedral shape of those particles possessing a FCC structure. Based on the geometrical consideration, Ino discussed the stability of MTPs comprising icosahedrons and decahedrons in terms of the specific surface energy, the twin boundary energy, the elastic strain energy, and the adhesive energy to the substrate. The occurrence of MTPs is now a common phenomenon in nanoparticles with FCC structure. Correspondingly, the MTP model gives us an account of the existing behavior in morphologies of mesoporous materials. Namely, icosahedral and decahedral shapes are expected to consist of twin-related tetrahedrons packed along (111) faces. In the case of an icosahedron, for instance, the whole structure contains one primary, three secondary, six tertiary, six quartic, three quintic, and one sextic tetrahedral units (see Figure 4b). Representations of the other shapes are shown in Figure 4c–e.

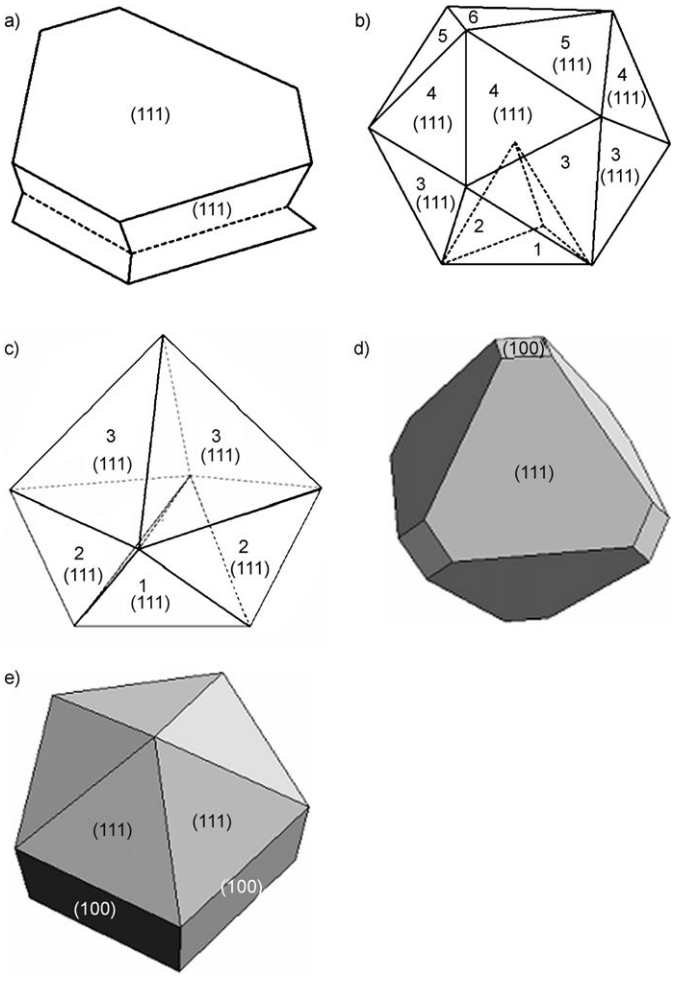

Figure 4. Schematic representations with Miller indices for the morphologies discussed. a) Triangular plate type; the dotted line represents a twin boundary. b) MTPs forming an icosahedron composed of 20 tetrahedrons, where the numbers specify the multiplicity of the twinning starting with the tetrahedron at the bottom. c) MTPs forming a decahedron composed of 5 five tetrahedrons. The multiplicity is indicated likewise. d) Wulff polyhedral single crystal. e) D-Wulff polyhedron.

Since the discovery of MTPs, various theoretical and experimental investigations have been reported[12] and different types of mechanisms have been proposed. As an example, Marks commented that the nucleation and growth of the particle are dominated by the probability of morphologies at a given condition, and are thus history-dependent.[13] In general, MTPs are not capable of growth to a large size because of the internal elastic strain arising from angular misfits of tetrahedral single crystals. According to the original evaluation by Ino,[14] it was suggested that the icosahedral MTP is the most stable in the region where the length of one edge r is short enough, while the energy rapidly increases with increasing r because of the internal elastic strain from misfits between tetrahedral building units. Thus, the particle size of icosahedrons should be smaller than that of decahedrons. Our SEM observations agree with this evaluation, as we observed that icosahedrons tended to be smaller compared to decahedrons. Meanwhile, the plate-type particle grows two dimensionally parallel to the twin boundary, and ends up with a variation of particle sizes.

The effect of the number of constituents (N) on the stability of MTPs should be discussed. The MTPs of the silica mesoporous crystal show a remarkably large N in comparison with those of FCC metals. Simple geometrical consideration gives the estimated value of N for both icosahedrons and decahedrons, since the relation between the edge length (r) of a tetrahedron built with a single FCC structure and a unit cell parameter (a) of the FCC lattice can be expressed by $N = \sqrt{2}r^3/3a^3$. In our case of an icosahedron composed of 20 tetrahedrons and a decahedron composed of 5 tetrahedrons, N is expected to be approximately 10^9, while $N < 10^5$ for Au MTPs as an example. This finding suggests that surfactant micelles are more flexible constituents compared with metal atoms, which can compensate the internal strain energy during the formation of MTPs. In this respect, the effect of HCP stacking arising from twinnings on measured XRD patterns is suppressed, because the number of FCC constituents exceeds hexagonal close packing by $r^{3/2}$ as r increases.

The use of gemini surfactant generally affords the SBA-2 type of structure as a mixture of 3D hexagonal and $Fm\bar{3}m$ symmetry.[15] However, the pure $Fm\bar{3}m$ mesostructure was

achieved under extremely low reactant concentrations starting with a clear solution (see Experimental Section). Synthesis under low-concentration conditions would make micelles in the solution more diffuse, and crystallization more kinetically controlled. As suggested from the reconstructed 3D structure, the shape of the micelles is highly spherical. By analogy with metal nanoparticles, we speculate that such a spherical shape of the surfactant aggregates should be a key to open the door to a pure FCC phase and the occurrence of multiple twinning during self-assembly with silica precursors. Although the formation energy of CCP stacking would be expected to be close to that of HCP stacking, our results suggested that micellar constituents should prefer to stack not by hexagonal close packing but by cubic close packing. This evokes the notion that the particle morphologies result in an icosahedral or decahedral shape with multiple twinning, and a triangular plate with single twinning.

Finally, MTPs can give 10-fold symmetry in their diffraction patterns as well as quasi-crystals, and thus the structural determination of quasi-crystals would be difficult using only diffraction techniques. As the existence of quasi-crystals in the liquid-crystalline phase (liquid quasi-crystals) has been revealed recently for 12-fold symmetry,[16] further discussions are required to clarify liquid quasi-crystals on the mesoscopic scale.[17]

Experimental Section

Mesoporous silica was synthesized by using gemini surfactant $[C_{16}H_{33}N(CH_3)_2(CH_2)_3(CH_3)_3N]Br_2$ (termed $C_{16\text{-}3\text{-}1}$) and tetraethyl orthosilicate (TEOS; from China Chemical Reagent Corporation) as a silica source in the presence of sulfuric acid.

Synthesis of mesoporous silica: The surfactant $C_{16\text{-}3\text{-}1}$, distilled water, and sulfuric acid were mixed to obtain a homogeneous solution, which was allowed to react at 0 °C prior to the addition of the silica source TEOS. After the addition of TEOS, the mixture was stirred for 3 min and then the reaction was continued at 0 °C under static conditions for 3 days. The resultant white precipitate was isolated by filtration (without washing) and dried at 100 °C overnight. The as-synthesized sample was calcined in air under static conditions at 630 °C for 4 h. The molar composition of the $C_{16\text{-}3\text{-}1}$/TEOS/H_2SO_4/H_2O reaction mixture was 1:10:160:8000.

Characterization: The powder XRD pattern of the mesoporous silica was recorded on a STOE STADI powder diffractometer with $Cu_{K\alpha 1}$ (wavelength 1.5406 Å) radiation in the step-scan mode with tension = 40 kV and current = 50 mA. The rate of the measuring step was 0.02° min^{-1}. The scan range was $2\theta = 1.0$–8.0°.

Nitrogen adsorption–desorption measurements were conducted at −196 °C on an ASAP2020 Micromeritics instrument. The sample was outgassed for 6 h at 200 °C. The BET surface area was calculated from the relative pressure range of 0.05–0.20 on the adsorption branch. The total pore volume was estimated from the amount adsorbed at a relative pressure of 0.96. The pore-size distribution was analyzed using nonlocal density functional theory assuming the Tarazona model.

A JEOL JEM-2000FX microscope was used to obtain both HRTEM images and ED patterns at an accelerating voltage of 200 kV. The spherical aberration, convergence of angle, and spread of defocus were 1.00 mm, 0.50 mrad, and 80.00 Å, respectively. Images were recorded with a CCD camera (model Keen View, SIS analysis) with an image size of 1376 × 1032 pixels (pixel size = 23.5 × 23.5 μm^2). The observation was carried out at × 40000–120000 magnification under low-dose conditions of beam intensity.

After spattering gold particles on the specimen, SEM images were recorded by a JEOL 820 instrument operating at an accelerating voltage of 5 kV.

A 3D reconstruction technique using the HRTEM images obtained was carried out on the basis of the Fourier analysis, which enabled us to look into the features of the structure involved. CRISP (Calidris, version 2.1a) and Mathematica (Wolfram Research, version 5.0) software were used to extract FCs from the HRTEM images and for Fourier synthesis of FCs, respectively.

Received: April 12, 2006
Revised: July 7, 2006
Published online: September 5, 2006

Keywords: crystal growth · electron microscopy · mesoporous materials · silica · surfactants

[1] J. M. Kim, S. K. Kim, R. Ryoo, *Chem. Commun.* **1998**, 259.
[2] S. Guan, S. Inagaki, T. Ohsuna, O. Terasaki, *J. Am. Chem. Soc.* **2000**, *122*, 5660.
[3] O. Terasaki, T. Ohsuna; Z. Liu, Y. Sakamoto, A. E. Garcia-Bennett, *Stud. Surf. Sci. Catal.* **2004**, *148*, 261.
[4] a) S. Che, S. Kamiya, O. Terasaki, T. Tatsumi, *J. Am. Chem. Soc.* **2001**, *123*, 12089; b) S. Kamiya, H. Tanaka, S. Che, T. Tatsumi, O. Terasaki, *Solid State Sci.* **2003**, *5*, 197; c) S. Che, H. Li, S. Lim, Y. Sakamoto, O. Terasaki, T. Tatsumi, *Chem. Mater.* **2005**, *17*, 4103.
[5] S. Che, S. H. Lim, M. Kaneda, H. Yoshitake, O. Terasaki, T. Tatsumi, *J. Am. Chem. Soc.* **2002**, *124*, 13962.
[6] C. Yu, B. Tian, J. Fan, G. D. Stucky, D. Zhao, *J. Am. Chem. Soc.* **2002**, *124*, 4556.
[7] S. Che, Y. Sakamoto, O. Terasaki, T. Tatsumi, *Microporous Mesoporous Mater.* **2005**, *85*, 207.
[8] a) A. Carlsson, M. Kaneda, Y. Sakamoto, O. Terasaki, R. Ryoo, S. H. Joo, *J. Electron Microsc.* **1999**, *48*, 795; b) Y. Sakamoto, M. Kaneda, O. Terasaki, D. Zhao, J.-M. Kim, G. D. Stucky, H. J. Shin, R. Ryoo, *Nature* **2000**, *408*, 449.
[9] Q. Huo, R. Leon, P. M. Petroff, G. D. Stucky, *Science* **1995**, *268*, 1324.
[10] Y. Sakamoto, I. Diaz, O. Terasaki, D. Y. Zhao, J. Perez-Pariente, J. M. Kim, G. D. Stucky, *J. Phys. Chem. B* **2002**, *106*, 3118.
[11] S. Ino, *J. Phys. Soc. Jpn.* **1966**, *21*, 346.
[12] N. Doraiswamy, L. D. Marks, *Philos. Mag. B* **1995**, *71*, 291.
[13] L. D. Marks, *Rep. Prog. Phys.* **1994**, *57*, 603.
[14] S. Ino, *J. Phys. Soc. Jpn.* **1969**, *27*, 941.
[15] W. Zhou, H. M. A. Hunter, P. A. Wright, Q. Ge, J. M. Thomas, *J. Phys. Chem. B* **1998**, *102*, 6933.
[16] X. B. Zeng, G. Ungar, Y. S. Liu, V. Percec, A. E. Dulcey, J. K. Hobbs, *Nature* **2004**, *428*, 157.
[17] A. E. Garcia-Bennett, N. Kupferschmidt, Y. Sakamoto, S. Che, O. Terasaki, *Angew. Chem.* **2005**, *117*, 5451; *Angew. Chem. Int. Ed.* **2005**, *44*, 5317.

